Soil Dynamics and Earthquake Engineering 29 (2009) 1220–1235

Contents lists available at ScienceDirect

Soil Dynamics and Earthquake Engineering

journal homepage: www.elsevier.com/locate/soildyn

A simplified method for unified buckling and free vibration analysis of pile-supported structures in seismically liquefiable soils

S. Bhattacharya [a,*], S. Adhikari [b], N.A. Alexander [c]

[a] Department of Civil Engineering, University of Bristol, Room no. 2.37, Queens Building, Bristol BS8 1TR, United Kingdom
[b] Aerospace Engineering, University of Swansea (Wales), Singleton Park, Swansea SA2 8PP, United Kingdom
[c] Structural Engineering, University of Bristol, Room no 2.33, Queens Building, Bristol BS8 1TR, United Kingdom

ARTICLE INFO

Article history:
Received 6 October 2008
Received in revised form
27 January 2009
Accepted 29 January 2009

Keywords:
Piles
Earthquake
Liquefaction
Elasto-dynamics
Buckling
Lateral spreading
Frequency
Soil–structure interaction

ABSTRACT

In seismic-prone zones with liquefiable deposit piles are routinely used to support structures (buildings/bridges). In this paper, a unified buckling and dynamic approach is taken to characterize this vibration. The pile–soil system is modelled as Euler–Bernoulli beam resting against an elastic support with axial load and a pile head mass with rotary inertia. The emphasis here is to obtain a simple expression that can be used by practicing engineers to obtain the fundamental frequency of the structure–pile–soil system. An approximate method based on an equivalent single-degree-of-freedom model has been proposed. Natural frequencies obtained from the exact analytical method are compared with approximate results. Proposed expressions are general as they are functions of non-dimensional parameters. It is shown that this simplified method captures the essential design features such as: (a) the continuous reduction of the first natural frequency of the structure–pile–soil system due to progressive reduction of soil stiffness due to liquefaction; (b) the reduction in the axial load-carrying capacity of the pile due to instability caused by liquefaction. The results derived in this paper have the potential to be directly applied in practice due to their simple yet general nature. An example problem has been taken to demonstrate the application of the method.

1. Introduction

1.1. An overview on the collapse of pile-supported structures

Collapse and/or severe damage of pile-supported structures are still observed after strong earthquakes despite the fact that a large factor of safety against axial capacity and bending due to lateral loads is employed in their design. Fig. 1(a) shows a pile-supported structure following the 1995 Kobe earthquake. Fig. 1(b), on the other hand, shows a schematic diagram of the same building along with the location of the cracks in the pile. All design codes employ a large margin of safety against the hinge formation (using partial factors), yet occurrences of pile failure due to liquefaction are abundant. This is strong evidence that there are perhaps other mechanisms governing these failures, which the code does not consider. A critical review of the current theories of pile failure and the hypothesis behind the current codes of practice can be found in [10].

1.2. Bending mechanism due to kinematic loads on the pile and inertia of the superstructure

The current understanding of pile failure as hypothesised by some codes of practice is as follows: in an earthquake if loose sands are saturated, they lose strength as excess pore water pressure is generated and the soil tends to liquefy. This means that if the soil is on a slope, it will flow downslope, which is often termed as *lateral spreading*. Up to now it has been assumed that the failure of these buildings was caused by the lateral pressure of the flow of the liquefied sand and any non-liquefied stabilised crust resting on the top of the liquefied soil (see for example [1–3,8,18,19,21–25,27,28,40,41,45,47]). Fig. 2 explains the hypothesis of failure. This mechanism is therefore based on kinematic bending failure; see [28]. The movement of the superstructure i.e. inertia force can also induce bending moments in the pile. The effects of inertia of the superstructure on the pile stresses are considered separately in [28]. They are not combined with the kinematic bending moments and the explanation can be found in [27]. Eurocode 8 advises designers to design piles against bending due to inertia and kinematic forces arising from the deformation of the surrounding soil. Other codes, such as NEHRP code and Indian Code [IS 1893, 2002] also focus on bending strength of the pile. In summary, the current understanding of pile failure simply

* Corresponding author.
E-mail addresses: S.Bhattacharya@bristol.ac.uk, subhamoy.bhattacharya@gmail.com (S. Bhattacharya).

0267-7261/$ - see front matter Crown Copyright © 2009 Published by Elsevier Ltd. All rights reserved.
doi:10.1016/j.soildyn.2009.01.006

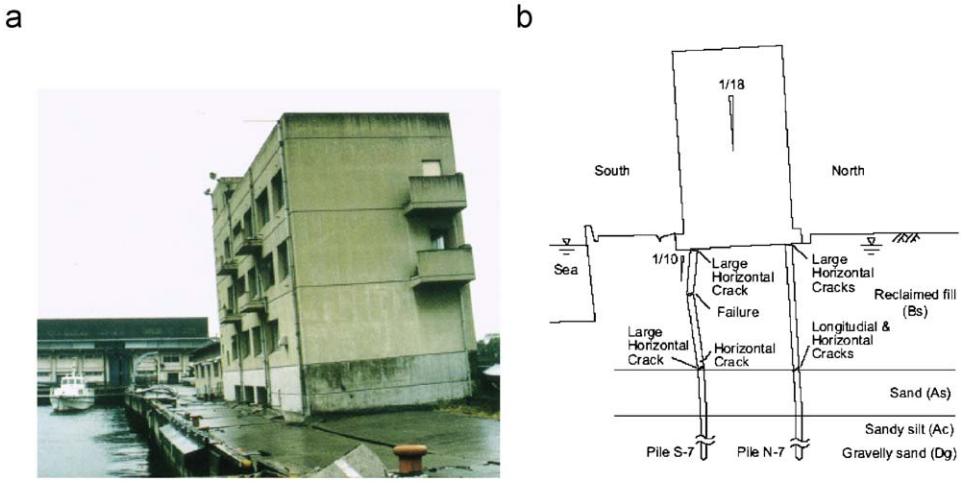

Fig. 1. (a) Tilting of a pile-supported building following the 1995 Kobe earthquake; (b) formation of crack. Photo courtesy K. Tokimatsu and Ref. [14].

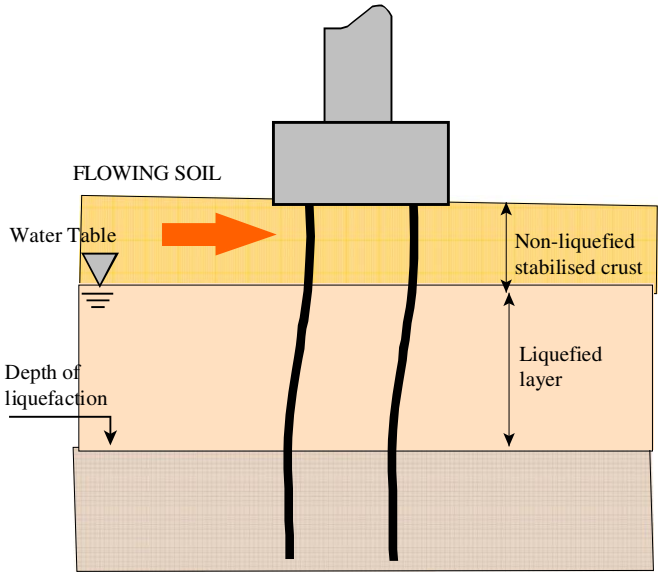

Fig. 2. Current understanding of pile failure.

treats piles as beams and assumes that the lateral loads due to inertia and soil movement cause bending failure of the pile. The stability issue due to the axial loads acting on the pile at all times and dynamic considerations are not taken into account.

1.3. Buckling mechanism arising due to unsupported length of the pile in liquefiable zone

A recent investigation by Bhattacharya et al. [11–13] conclusively showed that a pile becomes laterally unsupported in the liquefiable zone during strong shaking that led to another failure mechanism. The soil around the pile liquefies and loses much of its stiffness and strength, so the piles now act as unsupported long slender columns and simply buckle under the action of the vertical superstructure (building) loads. Therefore, this hypothesis is based on a buckling mechanism that has later been verified by other researchers; see for example [29–31,46,48]. Bhattacharya et al. [12] analysed 14 case histories of pile foundation performance based on buckling parameters. Though buckling mechanism can classify these pile failures, the location of hinge formation/cracks in the piles as observed in field survey cannot be explained by buckling instability theory. Criticisms of buckling mechanism can be found in [44]. This led to the search of any other mechanism of failure.

1.4. Unified buckling mechanism and dynamic (resonance-type) failure

Structurally, buckling of a slender column can be viewed as a complete loss of lateral stiffness to resist deformation. It is commonly known as an instability phenomenon. During liquefaction, if a pile buckles it can be concluded that the lateral stiffness of the pile is lost. From a dynamics point of view, as the applied axial load approaches the buckling load it can also be observed that the fundamental natural frequency of the system drops to zero [39]. Essentially, at the point where the natural frequency drops to zero, the inertial actions on the system no longer contribute. Thus, the system's dynamical equations of motion degenerate into a statics stability problem. During seismic liquefaction, the axial load on the pile in the liquefied zone increases due to the loss of shaft resistance. Due to this extra axial load, the stiffness of the pile–soil system reduces and so does the vibration frequencies. At the point of instability the fundamental vibration mode and buckling mode shapes are identical. Thus, as the soil transforms from solid to a fluid-like material i.e. from partial-liquefaction stage to full-liquefaction stage, the modal frequencies and shapes of the pile change.

Considering the first natural frequency of the pile–soil–superstructure system, it is suggested that the "other mechanism" may probably be the two effects arising from the removal of the lateral support the soil offers to the pile while in liquefied state. They are: (a) increase in axial load in the pile in the potentially unsupported zone due to loss of shaft resistance; (b) dynamics of pile-supported structure due to frequency-dependent force arising from the shaking of the bedrock and the surrounding soil than can cause dynamic amplification of pile head displacements leading to resonance-type failure.

1.5. Winkler models for liquefied soil

Beam on Non-linear Winkler foundation (BNWF) or "*p–y*" method is commonly used to analyse piles [7,17]. In "*p–y*" method, the soil is modelled as non-linear springs where '*p*' refers to the lateral soil pressure per unit length of pile and the '*y*' refers to the

lateral deflection. Fig. 3 shows a particular p–y model for non-liquefied soil and its corresponding liquefied condition based on an empirical method. The reduction of strength is carried out using p-multiplier and typical values of this multiplier can be found in [5,37,32]. It may be noted that the initial stiffness (i.e. the initial slope of p–y curve) degrades when the soil transforms from being solid to fluid. A detailed discussion on the shape of p–y curves for liquefied soil can be found in [16]. However, analysis of the full-scale tests such as Rollins et al. [36], centrifuge tests such as Bhattacharya et al. [13], laboratory tests on liquefied soil by Yasuda et al. [43], 1-g pipe pulling tests, Takahashi et al. [38] suggests that the shape of the "p–y" curve for liquefied soil should look like an S curve. Fig. 4(a) shows the change of "p–y" curves when the soil is transformed from being solid to fluid-like medium. Fig. 4(b) shows the shape following [16]. Fig. 5 shows the implications of "p–y" curve on the small-vibration analysis of a pile-supported structure. The main parameters of a load–displacement (p–y curve) relationship are the stiffness and strength of liquefied soil. The stiffness of the soil, i.e. the initial tangent stiffness of "p–y" curve, is the resistance of soil to unit pile deformation. Under non-liquefied condition, when the differential soil–pile movement is small (i.e. the soil is not pushed to its full capacity), the resistance on pile depends on

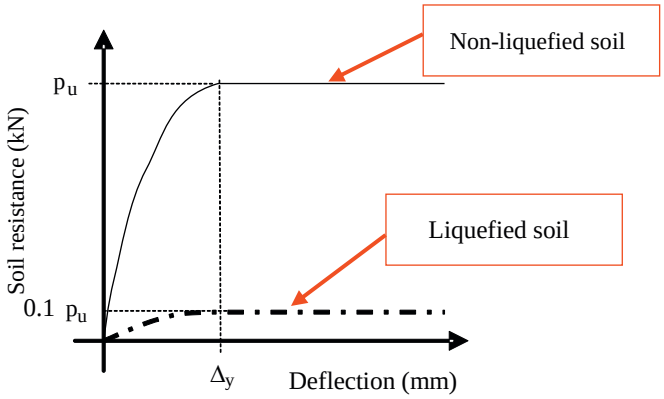

Fig. 3. p–y curve for non-liquefied soil and liquefied soil using p-multiplier.

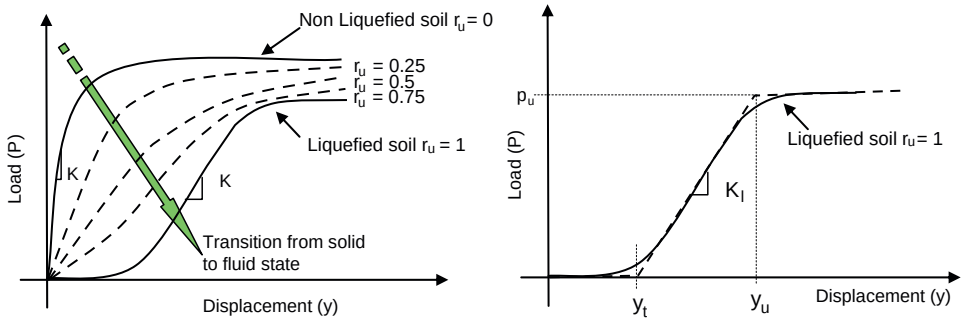

Fig. 4. (a) p–y curve for saturated sandy soil during the process of liquefaction ; (b) simplified p–y curve for liquefied soil [16].

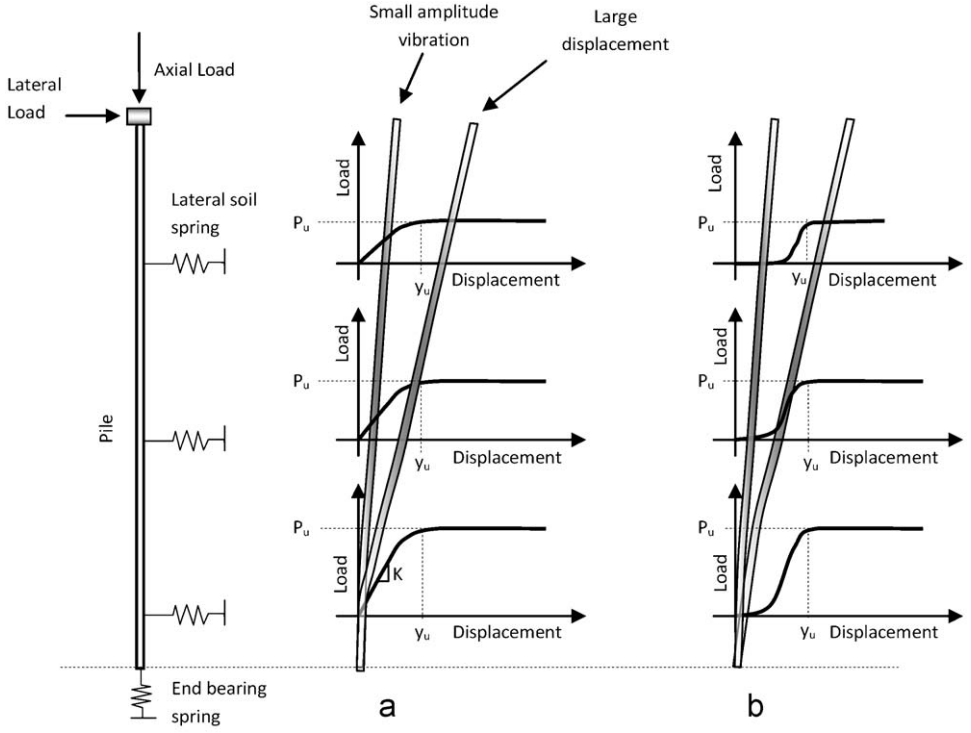

Fig. 5. Soil–pile interactions for two types of p–y curves (a) for non-liquefied case; (b) for liquefied case.

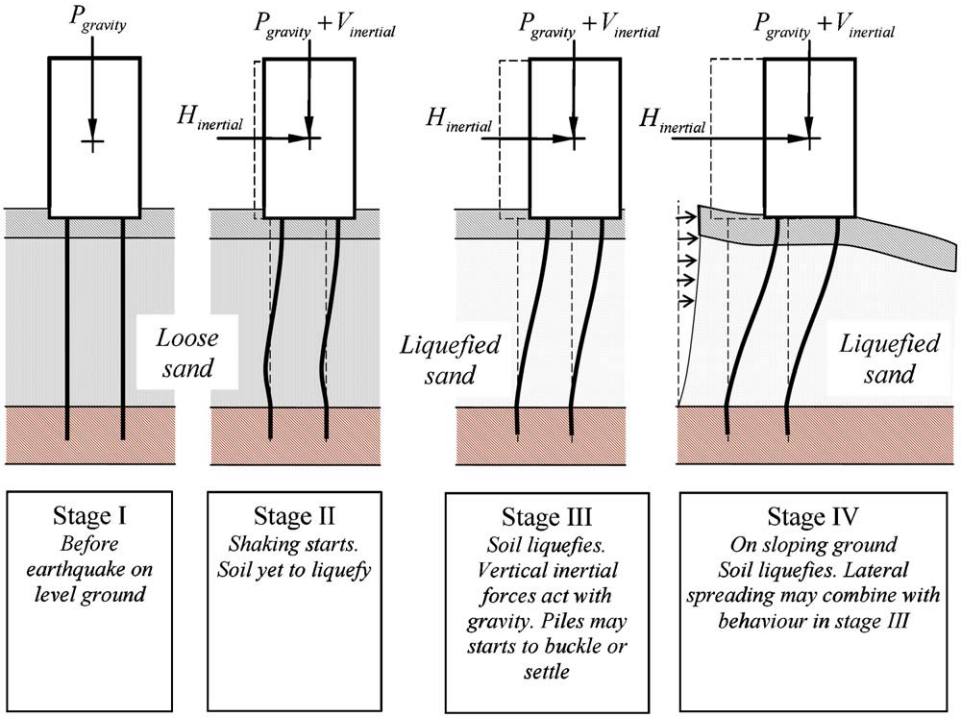

Fig. 6. Different stages of the loading.

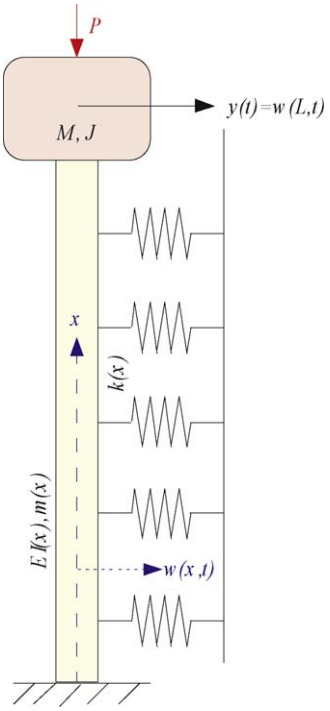

Fig. 7. Combined pile–soil model using Euler–Bernoulli beam with end mass and axial force.

the initial stiffness of the soil and the value of deflection (Fig. 5a). In contrast, the strength of soil is an important parameter while dealing with high-amplitude soil–pile interaction. In other words, when the differential soil–pile movement is large, the resistance offered by soil over pile is governed by the ultimate strength of the soil (Fig. 5a). For liquefied soil (see Fig. 5b), the pile response will be different for small and large amplitude vibrations. The lack of initial stiffness and strength of the liquefied soil will increase the P-delta effect for small amplitude vibration, and may promote buckling mode of failure of piles [4,11–13].

1.6. Aims and scope of this paper

Fig. 6 shows the different stages of loading of a pile-supported structure where the pile vibrates. In Stage II, when the soil has not fully liquefied, the transverse bending is expected to govern the internal stresses within the pile. As the liquefaction progresses, the coupled buckling (due to the unsupported length of the pile) and frequency-dependent resonance force would govern the internal stresses in the pile (Stage III). The key physical aspect that the authors aim to emphasize is that the motion of the pile (and consequently the internal stresses leading to the failure) is a coupled phenomenon. This coupling is, in general, non-linear and it is not straightforward to exactly distinguish the contributions of the different mechanisms towards an observed failure. It is, however, certainly possible that one mechanism may dominate over the others at a certain point of time during the period of earthquake motion and till the dissipation of excess pore water pressure. The purpose of this paper is therefore to understand the vibrational characteristics of the piled foundation at full liquefaction i.e. the time instant shown by Stage III in Fig. 6.

This paper is therefore aimed at explicitly quantifying the first natural frequency due to the effects of (1) axial force, (2) dynamic excitation and (3) reduction of the lateral support due to liquefaction. An attempt has been made to develop a simplified procedure. Essentially, the first natural frequency is derived based on an equivalent single-degree-of-freedom model. This new approach relies on the proposed "stiffness correction factor" and "mass correction factors" which are derived in this paper. The applicability of this method is demonstrated using the case history described in Fig. 1(a) and (b).

2. Exact analytical formulation

An Euler–Bernoulli beam, as shown in Fig. 7, is considered. It is assumed that the bending stiffness of the pile is EI and it rests against a uniform elastic support of stiffness k. The pile has a head mass (M) with rotary inertia J. The mass per unit length of the pile is m and r is the radius of gyration. The pile is subjected to a constant compressive axial load P. Using the Hamilton's principle, the equation of motion of the beam is given by the following fourth-order partial differential equation:

$$\frac{\partial^2}{\partial x^2}\left(EI\frac{\partial^2 w}{\partial x^2}\right)+\frac{\partial}{\partial x}\left(P\frac{\partial w}{\partial x}\right)-\frac{\partial}{\partial x}\left(mr^2\frac{\partial \ddot{w}}{\partial x}\right)+k\,w+m\,\ddot{w}=f(x,t) \tag{1}$$

where $w(x, t)$ is the transverse deflection of the beam and t the time, $\ddot{w}$ is the second derivative of w with respect to time i.e. acceleration, $P(x)$ is the axial load, mr^2 is the polar moment of inertia of the beam and $f(x, t)$ is a time-dependent load on the beam. The derivation of Eq. (1) from first principle can be found in [9]. A closed-form solution for Eq. (1) does not exist and therefore it is considered appropriate to solve the equation using numerical techniques for different boundary conditions at the top and bottom of the pile. As mentioned earlier, the first aim of this paper is to examine the change in the natural frequency of the piled foundation when the soil liquefies, i.e. when the support stiffness k reduces. For free vibration problem, $f(x, t)=0$. The four boundary conditions associated with this problem are expressed in Table 1.

Table 1
Boundary condition.

Deflection is zero at $x=0$	$w(0, t)=0$
Rotation is zero at $x=0$	$w'(0, t)=0$
Bending moment is zero at $x=L$	$EIw''(L, t)+J\ddot{w}'(L, t)=0$
Shear force is zero at $x=L$	$EIw'''(L, t)-Pw'(L, t)-M\ddot{w}(L, t)-J\ddot{w}'(L, t)=0$

Assuming harmonic solution and using separation of variables, the solution is of the form given by

$$w(x,t)=W(\xi)e^{i\omega t},\quad \xi=\frac{x}{L} \tag{2}$$

Substituting Eq. (2) in the equation of motion (Eq. (1)) results in Eq. (3). Note that primes now indicate derivatives with respect to ξ.

$$W''''+\left(\frac{PL^2}{EI}+\frac{mr^2L^2}{EI}\omega^2\right)W''-\left(\frac{mL^4}{EI}\omega^2-\frac{kL^4}{EI}\right)W=0 \tag{3}$$

It is convenient to express Eq. (3) in terms of non-dimensional parameters. The following non-dimensional parameters are introduced: axial force ν, Eq. (4), support stiffness η, Eq. (5), frequency parameter Ω, Eq. (6), mass ratio α, Eq. (7) and radius of gyration μ, Eq. (8). The definition of radius of gyration is given by Eq. (9).

$$\nu=\frac{PL^2}{EI} \tag{4}$$

$$\eta=\frac{kL^4}{EI} \tag{5}$$

$$\Omega^2=\omega^2 f_0^2,\quad f_0^2=\frac{mL^4}{EI} \tag{6}$$

$$\alpha=\frac{M}{mL} \tag{7}$$

$$\mu=\frac{r}{L} \tag{8}$$

$$r=\sqrt{\frac{I}{A}} \tag{9}$$

Thus, Eq. (3) can be re-expressed in non-dimensional form as shown in Eq. (10).

$$W''''+(\nu+\mu^2\Omega^2)W''-(\Omega^2-\eta)W=0 \tag{10}$$

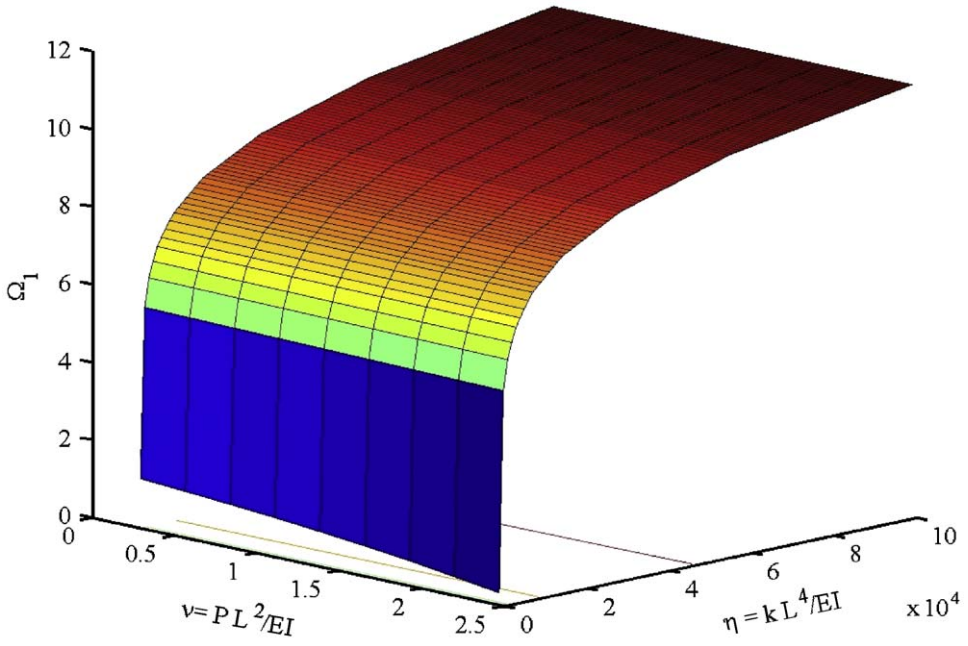

Fig. 8. Variation of first natural frequency.

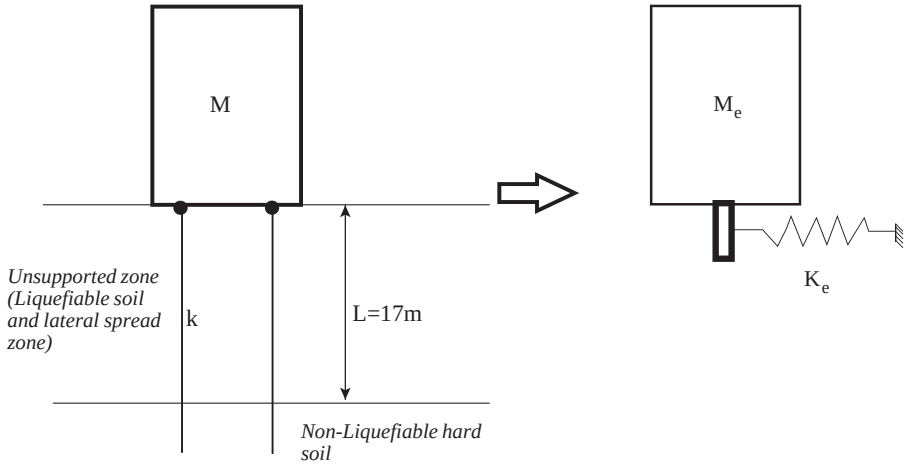

Fig. 9. Equivalent single-degree-of-freedom system.

The boundary conditions given by equations in Table 1 can also be transformed in terms of the non-dimensional parameters introduced above and the associated eigenvalue problem can be solved to obtain the natural frequencies of the system. The details of the solution procedure are given in [4]. It is necessary to mention that these equations are transcendental and very complex and therefore are solved numerically. Once the non-dimensional frequency Ω is obtained by solving these equations, the actual natural frequency of the piles can be obtained from Eq. (6). Appendix-A shows the complexity of the equation. Fig. 8 shows a typical result of the analysis where Ω_1 shows the non-dimensional first natural frequency for a range of non-dimensional axial load v and non-dimensional support stiffness η.

3. Approximate natural frequency based on equivalent SDOF assumption

In the previous section exact expressions for the equation of the natural frequencies of the combine pile–soil system have been derived. The transcendental equations are very complex running into six lines and therefore numerical solutions are the only options. In this section, an attempt has been made to derive approximate closed-form solution with the aim of gaining physical insights. For earthquake excitations, the first mode of vibration is most significant and therefore the focus of the study is on the first mode.

In the first mode, the distributed system can be replaced by a single-degree-of-freedom system with equivalent stiffness K_e and equivalent mass M_e as shown in Fig. 9. The first natural frequency is given by

$$\omega_1 = \sqrt{\frac{K_e}{M_e}} \tag{11}$$

Following [15] [Table 8-8, case 2, p 158] the equivalent mass of a cantilever is given by

$$M_e = M + 0.24M_b = (\alpha + 0.24)mL \tag{12}$$

For the case in hand, the cantilever beam apart from resting on elastic foundation also has an end force. Therefore, the coefficient 0.24 in Eq. (12) needs to be modified to take into account these effects. It is considered that the equivalent mass can be represented by

$$M_e = (\alpha + \gamma_m)mL \tag{13}$$

where γ_m is the *mass correction factor*.

Table 2
Boundary condition.

Deflection is zero at $x = 0$	$w(0) = 0$
Rotation is zero at $x = 0$	$w'(0) = 0$
Bending moment is zero at $x = L$	$w''(L) = 0$
Shear force is zero at $x = L$	$EIw'''(L) - Pw'(L) + F = 0$

Therefore, the first natural frequency can be expressed as

$$\omega_1 = \sqrt{\frac{K_e}{M_e}} = f_0\sqrt{\frac{3\gamma_k}{\alpha + \gamma_m}} \tag{14}$$

where the *stiffness correction factor* (γ_k) is defined in Eq. (15), K_{CL} is the equivalent stiffness of a cantilever beam (without lateral soil springs), f_0 the frequency scaling parameter is defined as before in Eq. (6)

$$\gamma_k = \frac{K_e}{K_{CL}}, \quad K_{CL} = \frac{3EI}{L^3} \tag{15}$$

The next step is therefore to obtain the values of γ_m and γ_k in terms of non-dimensional parameters.

3.1. Determination of the stiffness correction factor (γ_k)

The equivalent stiffness in the first mode is calculated by applying a unit static load to the free end of the pile and calculating the deflection under this load. For the static problem, the rotary inertia of the end mass and that of the pile can be neglected. The static equation and the associated boundary conditions can be obtained as a special case of Eq. (1).

$$EI\frac{\partial^4 w}{\partial x^4} + P\frac{\partial^2 w}{\partial x^2} + kw = 0 \tag{16}$$

The four boundary conditions associated with the above equation are expressed in Table 2. A constant static force F is applied at $x = L$.

Using non-dimensional length variable ξ and the transformation $w(x) = W(\xi)$, Eq. (16) becomes

$$W'''' + vW'' + \eta W = 0 \tag{17}$$

Eq. (17) can be solved using a trial solution $W(\xi) = e^{\lambda\xi}$. This results in the characteristic equation

$$\lambda^4 + v\lambda^2 + \eta = 0 \tag{18}$$

Solving quadratic Eq. (18) in λ^2 gives,

$$\lambda^2 = -\frac{v}{2} \pm \sqrt{\left(\frac{v}{2}\right)^2 - \eta} \tag{19}$$

Two cases may arise based on whether or not $\eta > (v/2)^2$

3.1.1. Case 1: $\eta > (v/2)^2$

For the problem in hand, the axial load is always compressive and therefore v is always positive. Under service condition (non-seismic and no liquefaction), $v < 1$ and both the roots become complex and can be expressed as

$$\lambda^2 = -\left(\frac{v}{2} + i\sqrt{\eta - \left(\frac{v}{2}\right)^2}\right), \quad -\left(\frac{v}{2} - i\sqrt{\eta - \left(\frac{v}{2}\right)^2}\right) \tag{20}$$

Using elementary algebra, the four roots of Eq. (20) can be expressed as

$$\lambda = \pm i\lambda_1 \pm \lambda_2 \tag{21}$$

where

$$\lambda_1 = \sqrt{\sqrt{\frac{\eta}{4}} + \frac{v}{4}} \quad \text{and} \quad \lambda_2 = \sqrt{\sqrt{\frac{\eta}{4}} - \frac{v}{4}} \tag{22}$$

In view of the roots obtained in Eq. (22), the solution $W(\xi)$ can be expressed as

$$W(\xi) = c_1 \sin(\lambda_1\xi)\sinh(\lambda_2\xi) + c_2 \cos(\lambda_1\xi)\sinh(\lambda_2\xi) + c_3 \sin(\lambda_1\xi)\cosh(\lambda_2\xi) + c_4 \cos(\lambda_1\xi)\cosh(\lambda_2\xi) \tag{23}$$

Applying the boundary condition (Table 2), the constants can be obtained. The deflection of the free-end δ_L can be obtained by substituting $\xi = 1$ and the equivalent stiffness can be obtained using Eq. (28).

$$K_e = \frac{F}{\delta_L} \tag{24}$$

The stiffness correction factor, γ_k, defined by Eq. (15) is given by Eq. (25). Necessary details of the method are given in Appendix B.

$$\gamma_k = (\lambda_1^2 + \lambda_2^2)(\lambda_1^2 + \lambda_2^2 + v) \times \frac{(\lambda_1^2 \cos 2\lambda_2 + \lambda_2^2 \cos 2\lambda_1) + (6\lambda_1^2\lambda_2^2 - \lambda_1^4 + v\lambda_1^2 - \lambda_2^4 - v\lambda_2^2)}{6\lambda_1\lambda_2(\lambda_1 \sin 2\lambda_2 - \lambda_2 \sin 2\lambda_1)} \tag{25}$$

The above expression of stiffness correction factor, γ_k, is quite general as it considers both the effect of axial load and support stiffness.

3.1.2. Case 2: $\eta \leqslant (v/2)^2$

This case may arise when η i.e. the soil stiffness is very small as can be expected near full liquefaction. In such cases, both the roots are real and negative and can be expressed as

$$\lambda^2 = -\left(\frac{v}{2} + \sqrt{\left(\frac{v}{2}\right)^2 - \eta}\right), \quad -\left(\frac{v}{2} - \sqrt{\left(\frac{v}{2}\right)^2 - \eta}\right) \tag{26}$$

Using elementary algebra, the four roots of equation can be expressed as

$$\lambda = \pm i\lambda_1, \quad \pm i\lambda_2 \tag{27}$$

where

$$\lambda_1 = \sqrt{\left(\frac{v}{2} + \sqrt{\left(\frac{v}{2}\right)^2 - \eta}\right)} \quad \text{and} \quad \lambda_2 = \sqrt{\left(\frac{v}{2} - \sqrt{\left(\frac{v}{2}\right)^2 - \eta}\right)} \tag{28}$$

Proceeding similarly as case 1, stiffness correction factor, γ_k, is given by Eq. (29) where numerator and denominator terms, γ_a and γ_b, respectively, are given in Eqs. (30) and (31).

$$\gamma_k = \frac{\gamma_a}{\gamma_b} \tag{29}$$

$$\gamma_a = \lambda_1^2\lambda_2^2(\lambda_2^2 + \lambda_2^2 - 2v)\sin\lambda_1 \sin\lambda_2 + \lambda_1\lambda_2(2\lambda_1^2\lambda_2^2 - v\lambda_1^2 - v\lambda_2^2)\cos\lambda_1 \cos\lambda_2 - \lambda_1\lambda_2(\lambda_2^4 - v\lambda_2^2 + \lambda_1^4 - v\lambda_1^2) \tag{30}$$

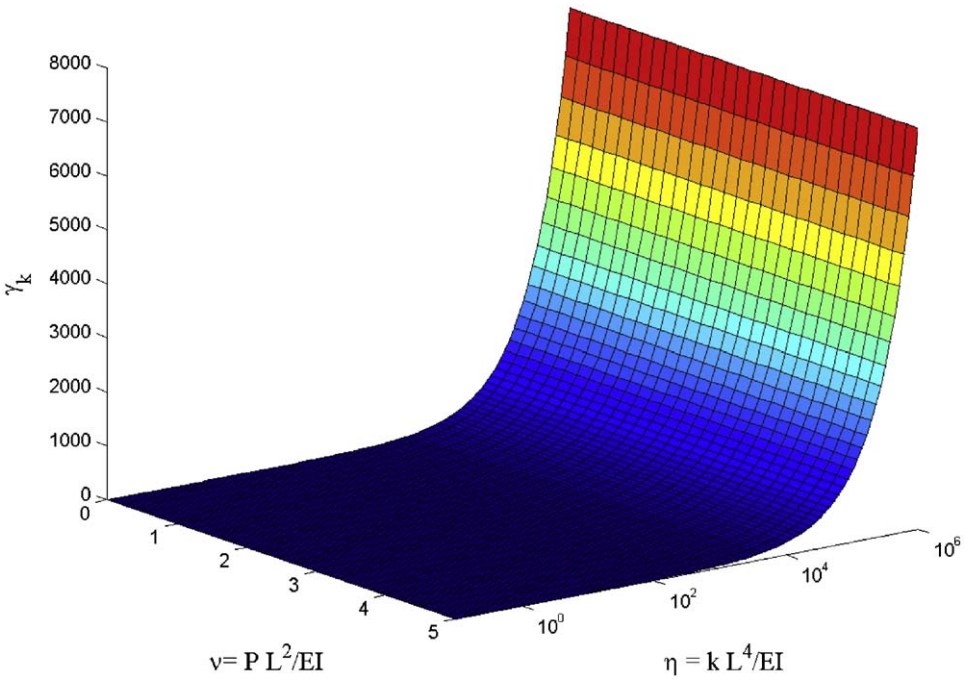

Fig. 10. Variation of the stiffness correction factor γ_k of a cantilever pile with respect to normalised support stiffness and axial load.

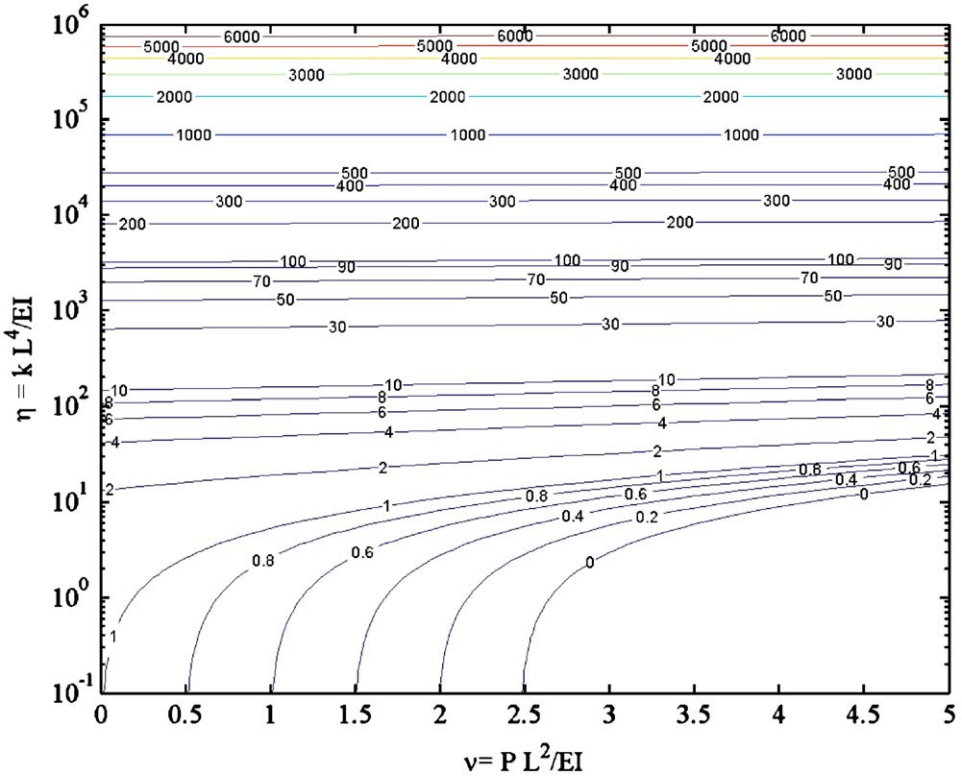

Fig. 11. Contour of the stiffness correction factor γ_k of a cantilever pile with respect to normalised support stiffness and axial load.

$$\gamma_b = 3(\lambda_2^2 - \lambda_1^2)(\sin\lambda_1 \cos\lambda_2 - \cos\lambda_1 \sin\lambda_2) \tag{31}$$

The value of γ_k given by Eqs. (25) and (29) cover the complete parametric space of η and ν. Fig. 10 shows the overall parametric variation of γ_k of a cantilever pile with respect to the normalised support stiffness, η, and axial load, ν. Fig. 11 shows the contour plot which can be used for approximate frequency calculation. Verification of the Eqs. (25) and (29) for well-known cases can be found in Appendix B.

3.2. Determination of the mass correction factor (γ_m)

From the physics of the problem it may be noted that the axial force within the beam will have very little influence on the equivalent mass. Therefore, neglecting the axial load, the equation of dynamic equilibrium can be expressed as

$$EI\frac{\partial^4 w}{\partial x^4} + kw + m\ddot{w} = 0 \tag{32}$$

To obtain the equivalent mass, we perturb the system by unit displacement amplitude at the free end so that $w(L) = 1$. Assuming standard harmonic solution as in Eq. (3), the equation of motion can be expressed as

$$W'''' + (\eta - \Omega^2)W = 0 \tag{33}$$

The boundary conditions are: $W(0) = 0$; $W'(0) = 0$; $W''(1) = 0$, $W(1) = 1$. Assuming the static deflected shape as the trial solution, $\Omega = 0$, and similar to the procedure used for solving Eq. (17), the following characteristic equation is obtained:

$$\lambda^4 + \eta = 0 \tag{34}$$

The solution of Eq. (34) is of the form

$$\lambda = (\pm 1 + i)\hat{\eta}, \quad \hat{\eta} = \frac{\sqrt[4]{\eta}}{\sqrt{2}} \tag{35}$$

Using the similar method as before and applying the boundary condition, the mass correction factor γ_m is obtained given by Eq. (36). The numerator and denominator terms are given by Eqs. (37) and (38), respectively. Details of the mathematics are given in Appendix C.

$$\gamma_m = \frac{\gamma_c}{\gamma_d} \tag{36}$$

$$\begin{aligned}\gamma_c = {} & 6\cos 2\hat{\eta}\sinh 2\hat{\eta} + 12\sinh 2\hat{\eta} + 3\sinh 4\hat{\eta} \\ & - 8\hat{\eta}\sinh 2\hat{\eta} - 3\sin 4\hat{\eta} - 12\sin 2\hat{\eta} + \\ & - 8\hat{\eta}\cosh 2\hat{\eta} - 6\cosh 2\hat{\eta}\sin 2\hat{\eta} + 8\hat{\eta}\cos 2\hat{\eta}\end{aligned} \tag{37}$$

$$\gamma_d = 8\hat{\eta}\cosh 4\hat{\eta} - 32\hat{\eta}\sin 2\hat{\eta}\sinh 2\hat{\eta} - 8\hat{\eta}\cos 4\hat{\eta} \tag{38}$$

Fig. 12 plots the parametric variation of the mass correction factor γ_m of a cantilever beam with respect to the normalised support stiffness. It is useful to note the special case when no lateral springs are present. Taking the limit $\hat{\eta} \to 0$, Eq. (36) turns out as

$$\lim_{\hat{\eta}\to 0}\gamma_m = \frac{33}{140} = 0.2357 \tag{39}$$

which agrees exactly with [15] [Table 8-8, case 1, p 158]. This analysis shows that the expression of γ_m is the generalisation of the classical case and the effect of elastic foundation is considered.

4. A case study to demonstrate the application of the simplified method

This section of the paper considers the piled foundation in Fig. 1(a) and (b) to demonstrate the application of the methodology illustrated in the previous section. The building was located 6 m from the quay wall on a reclaimed land in Higashinada-ku area of Kobe city. After the 1995 Kobe earthquake, the quay wall

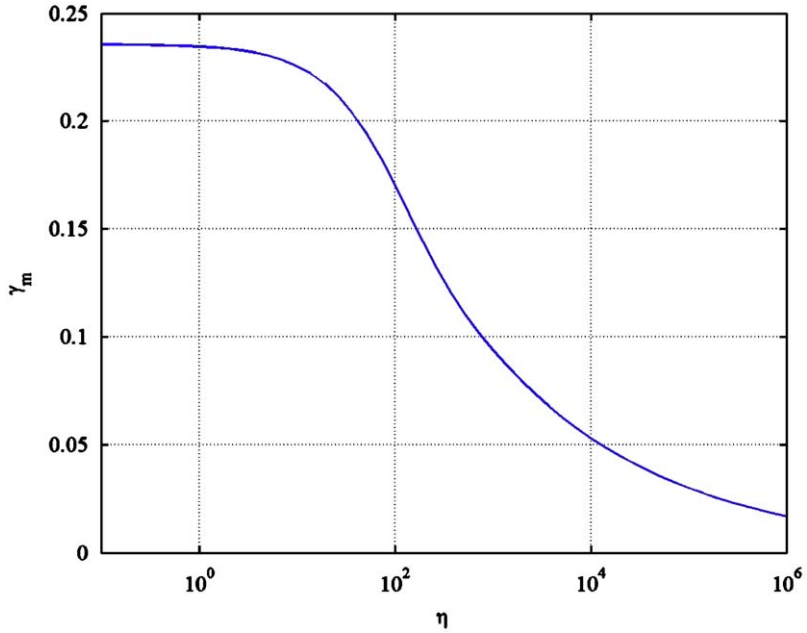

Fig. 12. Variation of the mass correction factor γ_m of a cantilever pile with respect to the normalised support stiffness.

Table 3
Design data of the building.

Building height	14.5 m above G.L.
Building dimensions	22.675 m × 7 m
Foundation type	Precast driven pile
Building type	R.C. framed
Number of stories	5
Axial load on each pile	412 kN
Dead load of the building	15,656 kN

Table 4
Design data of pile.

Length	20 m
External diameter	400 mm
Internal diameter	240 mm
Material	Prestressed concrete
E (Young's modulus)	30 GPa
EI	32.35 MN m^2

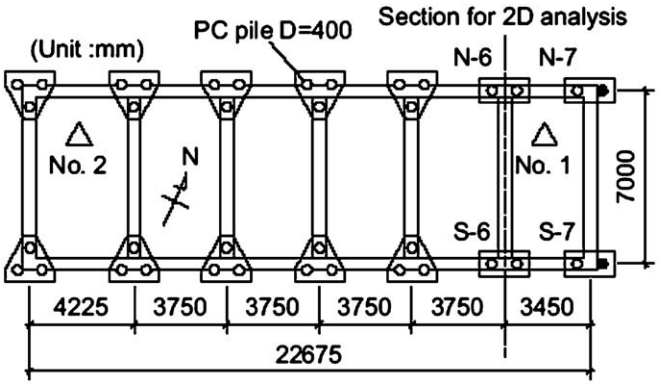

Fig. 13. Foundation plan showing the piles.

was displaced by 2 m towards the sea and the building tilted by 3°. Table 3 summarizes the design data of the building. Fig. 1(b) shows the post-earthquake failure investigation. The building was constructed in the early 1980s and was supported on 38 hollow, prestressed concrete piles. Table 4 summarizes the design data of the pile. The arrangement of the piles in the foundation is shown in Fig. 13. From the foundation plan, it is clear that the structure is moment-resisting RCC framed with tie beams at the foundation level. Fig. 14 shows the boring log of the site at locations. Input motion measured in the nearby Higashi-Kobe Bridge showed a peak ground acceleration of 0.38*g*. However, the PGA at the building site is not known. Extensive soil liquefaction and sand boils were observed in the area. The static axial load (P_{static}) acting in the building is reported to be 412 kN [42].

4.1. Liquefaction and site response analysis

The water table at the site was located 2 m below the ground level. It has been reported that 10 m of soil liquefied and therefore, the depth of liquefaction is 12 m. The boring log (Fig. 14) also suggests that the soil below the liquefied layer between 12 and 15 m consists of sandy silt (A_C) and has very low strength. This layer is composed of a clayey soil and it is most likely that it did not liquefy. However, the SPT value is less than 3 and no fixity against the lateral load can be expected from this layer. It can therefore be inferred that the plane of fixity of the pile against lateral loads after full liquefaction will be few pile diameters below 15 m. In the present study, this depth has been considered to be 17 m.

4.2. Effect of the non-liquefied crust

Where piles of diameter *D* pass through a depth more than 5*D* of stiff non-liquefiable soil, it would not be unreasonable to take that portion of the pile as being restrained against rotation. If the portion passing through 5*D* of stiff soil is at the pile toe, and there is no lower layer of liquefied material, the toe could be regarded also as being fixed in location. In addition to the fixity at the pile toe, if the non-liquefied crust above the liquefiable soil was somehow prevented from sliding, as in the rather unlikely scenario in the case of earthquakes, the pile can be best regarded as completely fixed at both ends. In the building under

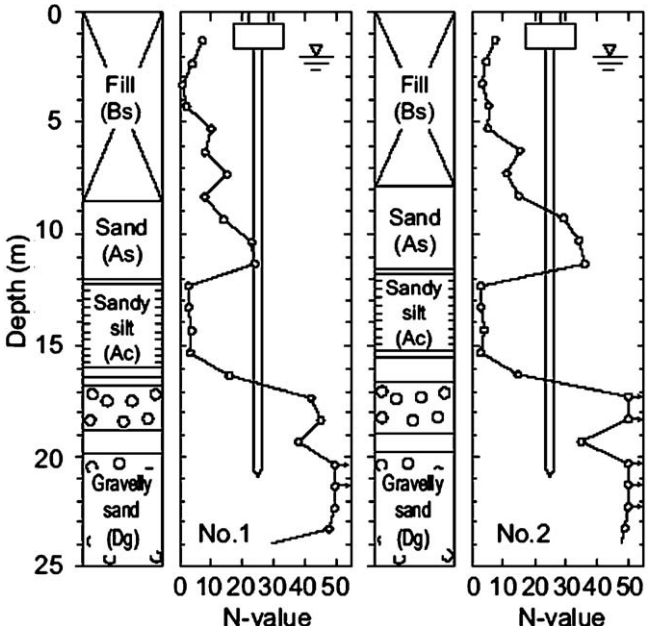

Fig. 14. Boring log of the soil at two locations at the site.

consideration, even though the pile passes through $5D$ in the crust, the non-liquefied crusts spread laterally, see Fig. 1(a) and (b). It must therefore follow that no restraint can be offered against sway of the pile crest.

Traditionally, the fundamental vibration period of RCC buildings are estimated by internationally calibrated data proposed by Structural Engineering Association of California (SEAOC) based [6]. The approximate fundamental natural period of vibration (T_a), in seconds, of a moment-resisting frame building with brick infill panels may be estimated by Eq. (40) or (41).

$$T_a = \frac{0.09H}{\sqrt{d}} \tag{40}$$

where H is the height of the building, in m. For the building under consideration, the height is 14.5 m; d is the base dimension of the building at the plinth level, in m, along the direction of the lateral force which is 7 m for the building. The time period based on Eq. (40) has been calculated to be 0.49 s.

Eurocode EC8 [20] suggests

$$T_0 = 0.05H^{0.75} \tag{41}$$

This is quite similar to the well-known equation of time period calculation $T = 0.1n$ where "n" is the number of storey. For 14.5 m high building, the number of storey can be considered to be about 5.

The non-dimensional parameters for analysis are:

Estimation of k in Eqs. (5) and (6) i.e. pile–soil stiffness is very uncertain. There are various practical methods to obtain these values:

1. API [7] approach: in this approach the stiffness (k) can be obtained by calculating the initial slope of the p–y curve. The well-known API p–y sand curve expression is given by Eq. (42) where k_1 is the modulus of subgrade reaction (F/L^3), h is depth, P_u is the ultimate resistance at depth h and A is a constant depending on the depth.

$$p = AP_u \tanh\left(\frac{k_1 h}{AP_u} y\right) \tag{42}$$

2. Elastic method pioneered by Rossett [35], Novak et al. [34] and later by Mylonakis [33].

Table 5
Non-dimensional values.

Parameters		Remarks
Mass ratio: mass of the building to the total mass of the piles (38 piles).	$\alpha = (M/38mL) = (15{,}656\,\text{kN}/(38 \times 40.2\,\text{kN})) = 10.2$	Where m = mass per unit length of the pile 204 kg/m.
Axial load ratio	$v = (PL^2/EI) = (412\,\text{kN} \times 17^2\,\text{m}^2/(32.35 \times 10^3\,\text{MN m}^2)) = 3.68$	
Frequency scaling parameters	$f_0 = \sqrt{EI/mL^4} = 1.37\,\text{Hz}$	

3. Terzaghi [49] approach: k is given by $k = E_S/1.35$, E_S being the elastic modulus of the soil.
4. AIJ [5] approach: is empirically similar to that of API [7].

These approaches give different values of pile–soil stiffness, i.e. k and therefore different values of time period of the building under normal condition (no earthquake). For example, API [7] approach gives a value of 0.2 s whereas the time period predicted by Eqs. (40) and (41) is about 0.5 s. To harmonise the value of initial pile–soil stiffness i.e. η parameter (Eq. (6)), it is proposed to back-calculate the value of k assuming the initial time period of vibration. Eq. (14) can be used for this purpose where ω_{NL} denotes frequency under non-liquefied condition.

$$\omega_{NL} = \frac{2\pi}{T_a} = \frac{2\pi}{0.49} = f_0\sqrt{\frac{3\gamma_k}{\alpha + \gamma_m}} \tag{43}$$

Taking appropriate values from Table 5 and taking γ_m as 0.02, the stiffness correction factor, γ_k before liquefaction can be estimated from Eq. (43). The obtained value is about 286. This signifies that the soil before liquefaction offers about 286 times more stiffness that the cantilever column fixed at the base. Also, this means the value of η is about 10^4.

4.3. Post-liquefaction building time period

AIJ [5] code, Ishihara [27] suggest that the value of soil stiffness drops to 0.1% in laterally spreading soil. Therefore η comes close to 100. Based on the contour plots (Figs. 11 and 12)

$$\gamma_m = 0.16, \quad \gamma_k = 7 \tag{44}$$

The circular frequency under fully liquefied condition (ω_L) can be estimated by

$$\omega_L = f_0\sqrt{\frac{3\gamma_k}{\alpha + \gamma_m}} = 1.37\sqrt{\frac{3 \times 7}{10.2 + 0.16}} = 1.95\,\text{rad s}^{-1} \tag{45}$$

Therefore, time period of the building at full liquefaction is about 3.2 s.

4.4. Discussion on the analysis results

The study showed that the time period of the building increased by about six times as soil fully liquefied. Therefore, the base shear of the building will decrease if shaking continues following liquefaction. Though the base shear may have reduced, it is the lever arm of the moment that will increase as the point of fixity of the pile is 17 m below G.L. Consequently, the dynamic axial load on the pile will increase. The designer therefore needs to check the bending moment of the pile under this loading scenario. It may be noted the simplified analysis carried out reduced the superstructure to a pile head mass.

5. Discussion and conclusions

Dynamic instability of pile-supported structures founded on liquefiable soils has been investigated. A coupled dynamical analysis combining (a) transverse bending, (b) dynamic buckling and (c) resonance motion has been carried out to comprehensively understand the failure mechanism of piles during an earthquake. In other words, bending, buckling and vibration are considered simultaneously to analytically model the pile–soil system. A distributed parameter model using the Euler–Bernoulli beam theory with axial load, support stiffness and end-mass with rotary inertia is considered. The non-dimensional parameters necessary to understand the dynamic instability are the non-dimensional axial force (v), non-dimensional soil stiffness (η), mass ratio between the building and the pile (α), non-dimensional radius of gyration of the pile (μ), and the non-dimensional rotary inertia of the building (β). An approximate method to obtain the fundamental natural frequency of the pile in liquefiable soils has been proposed.

The numerical results indicate that the first natural frequency of the structure reduces as the soil starts to lose its stiffness and is lowest when the soil is in the fully liquefied condition. Current codes of practice for piled foundations such as the Japanese code and the Eurocode are based only on the bending criteria where the lateral loads induce bending stress in the pile. It is well recognized that codes of practice have to specify some simplified approach for design which should provide a safe working envelope for any structure of the class being considered, and in full range of ground conditions likely to be encountered at different sites. The simplified approximate expressions are derived keeping this objective in mind. Since the first natural frequency of the system will start to drop when the soil transforms from being solid to liquid, it may come close to the excitation frequency of the earthquake motion (typically between 0.5 and 10 Hz). In such situations, the amplitude of vibration (and consequently the internal stresses) can grow significantly. Using the expressions derived in the paper, designers can estimate the first natural frequency at the full liquefaction and design the pile such that the resulting natural frequency does not come close to the expected frequency of the earthquake motion.

The approximation based on the equivalent SDOF system requires the calculation of the mass and stiffness correction factors. These correction factors take account of the axial force and soil stiffness. Explicit analytical expressions of the correction factors are derived in the paper. These results are general because they are in terms of the non-dimensional parameters of the building. An example problem has been considered to show the application of the method.

Acknowledgments

SA acknowledges the financial support of the UK Engineering and Physical Sciences Research Council (EPSRC) through the award of an Advanced Research Fellowship and The Leverhulme Trust for the award of the Philip Leverhulme Prize. SB acknowledges Somerville College, Oxford for the award of a Junior Research Fellowship.

Appendix A. Derivation of the frequency equations

Natural frequency of the pile-soil system are essentially the eigenvalues of Eq. (10). Here we derive the equations governing these eiganvalues. Assuming a solution of the form

$$W(\xi) = \exp\{\lambda\xi\} \tag{A.1}$$

and substituting in Eq. (10) results

$$\lambda^4 + \tilde{v}\lambda^2 - \left(\Omega^2 - \eta\right) = 0 \tag{A.2}$$

where

$$\tilde{v} = v + \mu^2\Omega^2 \tag{A.3}$$

Solving this equation for λ^2 we have

$$\begin{aligned}\lambda^2 &= \frac{\tilde{v}}{2} \pm \sqrt{\left(\frac{\tilde{v}}{2}\right)^2 + (\Omega^2 - \eta)} \\ &= -\left(\sqrt{\left(\frac{\tilde{v}}{2}\right)^2 + (\Omega^2 - \eta)} + \frac{\tilde{v}}{2}\right), \quad \left(\sqrt{\left(\frac{\tilde{v}}{2}\right)^2 + (\Omega^2 - \eta)} - \frac{\tilde{v}}{2}\right)\end{aligned} \tag{A.4}$$

Depending on whether $\Omega^2 - \eta > 0$ or not two cases arise.

Case 1: If $\tilde{v} > 0$ and $\Omega^2 - \eta > 0$ or $\Omega^2 > \eta$ then both roots are real with one negative and one positive root. Therefore, the four roots can be expressed as

$$\lambda = \pm i\lambda_1, \quad \pm\lambda_2 \tag{A.5}$$

where

$$\lambda_1 = \left(\sqrt{\left(\frac{\tilde{v}}{2}\right)^2 + (\Omega^2 - \eta)} + \frac{\tilde{v}}{2}\right)^{1/2} \tag{A.6}$$

and

$$\lambda_2 = \left(\sqrt{\left(\frac{\tilde{\nu}}{2}\right)^2 + (\Omega^2 - \eta)} - \frac{\tilde{\nu}}{2} \right)^{1/2} \tag{A.7}$$

In view of the roots in Eq. (A.5), the solution $W(\xi)$ can be expressed as

$$W(\xi) = c_1 \sin\lambda_1\xi + c_2 \cos\lambda_1\xi + c_3 \sinh\lambda_2\xi + c_4 \cosh\lambda_2\xi$$

or

$$W(\xi) = \mathbf{s}^T(\xi)\mathbf{c} \tag{A.8}$$

where the vectors

$$\mathbf{s}(\xi) = \{\sin\lambda_1\xi, \cos\lambda_1\xi, \sinh\lambda_2\xi, \cosh\lambda_2\xi\}^T \tag{A.9}$$

and

$$\mathbf{c} = \{c_1, c_2, c_3, c_4\}^T \tag{A.10}$$

Applying the boundary conditions in Table 1 on the expression of $W(\xi)$ in (A.8) we have

$$\mathbf{Rc} = \mathbf{0} \tag{A.11}$$

where the matrix

$$\mathbf{R} = \begin{bmatrix} s_1(0) & s_2(0) & s_3(0) & s_4(0) \\ s_1'(0) & s_2'(0) & s_3'(0) & s_4'(0) \\ s_1''(1) - \beta\Omega^2 s_1'(1) & s_2''(1) - \beta\Omega^2 s_2'(1) & s_3''(1) - \beta\Omega^2 s_3'(1) & s_4''(1) - \beta\Omega^2 s_4'(1) \\ s_1'''(1) + \tilde{\nu}s_1'(1) + \alpha\Omega^2 s_1(1) & s_2'''(1) + \tilde{\nu}s_2'(1) + \alpha\Omega^2 s_2(1) & s_3'''(1) + \tilde{\nu}s_3'(1) + \alpha\Omega^2 s_3(1) & s_3'''(1) + \tilde{\nu}s_3'(1) + \alpha\Omega^2 s_3(1) \end{bmatrix} \tag{A.12}$$

Substituting functions $s_j(\xi)$, $j = 1, \ldots, 4$ from Eq. (A.9) and simplifying we obtain

$$\mathbf{R} = \begin{bmatrix} 0 & 1 & 0 & 1 \\ \lambda_1 & 0 & \lambda_2 & 0 \\ -\sin(\lambda_1)\lambda_1{}^2 - \Omega^2\beta\cos(\lambda_1)\lambda_1 & -\cos(\lambda_1)\lambda_1{}^2 + \Omega^2\beta\sin(\lambda_1)\lambda_1 & \sinh(\lambda_2)\lambda_2{}^2 - \Omega^2\beta\cosh(\lambda_2)\lambda_2 & \cosh(\lambda_2)\lambda_2{}^2 - \Omega^2\beta\sinh(\lambda_2)\lambda_2 \\ -\cos(\lambda_1)\lambda_1{}^3 + \tilde{\nu}\cos(\lambda_1)\lambda_1 + \Omega^2\alpha\sin(\lambda_1) & \sin(\lambda_1)\lambda_1{}^3 - \tilde{\nu}\sin(\lambda_1)\lambda_1 + \Omega^2\alpha\cos(\lambda_1) & \cosh(\lambda_2)\lambda_2{}^3 + \tilde{\nu}\cosh(\lambda_2)\lambda_2 + \Omega^2\alpha\sinh(\lambda_2) & \sinh(\lambda_2)\lambda_2{}^3 + \tilde{\nu}\sinh(\lambda_2)\lambda_2 + \Omega^2\alpha\cosh(\lambda_2) \end{bmatrix}. \tag{A.13}$$

The constant vector in Eq. (A.11) cannot be zero for nontrivial solutions. Therefore, the equation governing the natural frequencies is given by

$$|\mathbf{R}| = 0$$

This, upon simplification reduces to

$$\begin{aligned} &\Big(-\sin(\lambda_1)\lambda_1^2\lambda_2\Omega^2\cosh(\lambda_2) + \lambda_1\Omega^2\cos(\lambda_1)\sinh(\lambda_2)\lambda_2^2 - \Omega^4\beta\ \sin(\lambda_1)\lambda_1^2\sinh(\lambda_2) \\ &\quad - \Omega^2\sin(\lambda_1)\cosh(\lambda_2)\lambda_2^3 + \Omega^4\sin(\lambda_1)\beta\ \sinh(\lambda_2)\lambda_2^2 + \cos(\lambda_1)\lambda_1^3\Omega^2\sinh(\lambda_2) \\ &\quad -2\ \lambda_1\Omega^4\cos(\lambda_1)\beta\ \cosh(\lambda_2)\lambda_2 + 2\ \Omega^4\lambda_2\beta\ \lambda_1\Big)\alpha + \Big(\lambda_1\lambda_2^3 - \cos(\lambda_1)\lambda_1\cosh(\lambda_2)\lambda_2^3 \\ &\quad -2\ \sin(\lambda_1)\lambda_1^2\sinh(\lambda_2)\lambda_2^2 - \lambda_1^3\lambda_2 + \cos(\lambda_1)\lambda_1^3\cosh(\lambda_2)\lambda_2\Big)\tilde{\nu} + \lambda_1^5\lambda_2 + \lambda_1\lambda_2^5 \\ &\quad + 2\ \cos(\lambda_1)\lambda_1^3\cosh(\lambda_2)\lambda_2^3 + \sin(\lambda_1)\lambda_1^4\sinh(\lambda_2)\lambda_2^2 - \sin(\lambda_1)\lambda_1^2\sinh(\lambda_2)\lambda_2^4 \\ &\quad - \sin(\lambda_1)\lambda_1^4\Omega^2\beta\ \cosh(\lambda_2)\lambda_2 - \Omega^2\beta\ \sin(\lambda_1)\lambda_1^2\cosh(\lambda_2)\lambda_2^3 - \Omega^2\beta\ \cos(\lambda_1)\lambda_1\sinh(\lambda_2)\lambda_2^4 \\ &\quad - \cos(\lambda_1)\lambda_1^3\Omega^2\beta\ \sinh(\lambda_2)\lambda_2^2 = 0. \end{aligned} \tag{A.15}$$

The natural frequencies can be obtained by solving Eq. (A.15) for Ω. Due to the complexity of this transcendental equation it should be solved numerically.

Case 2: If $\tilde{\nu} > 0$ and $\Omega^2 - \eta < 0$ or $\Omega^2 < \eta$ then both the roots are real and negative. Therefore, all of the four roots can be expressed as

$$\lambda = \pm i\lambda_1, \quad \pm i\widehat{\lambda}_2 \tag{A.16}$$

where λ_1 is as in the previous case

$$\lambda_1 = \left(\frac{\tilde{\nu}}{2} + \sqrt{\left(\frac{\tilde{\nu}}{2}\right)^2 - (\eta - \Omega^2)} \right)^{1/2} \tag{A.17}$$

and $\widehat{\lambda}_2$ is given by

$$\lambda_2 = \left(\frac{\tilde{\nu}}{2} + \sqrt{\left(\frac{\tilde{\nu}}{2}\right)^2 - (\eta - \Omega^2)}\right)^{1/2} \tag{A.18}$$

In view of the roots in Eq. (A.16), the solution $W(\xi)$ can be expressed as

$$W(\xi) = c_1 \sin\lambda_1\xi + c_2 \cos\lambda_1\xi + c_3 \sin\widehat{\lambda}_2\xi + c_4 \cos\widehat{\lambda}_2\xi$$

or

$$W(\xi) = \mathbf{s}^T(\xi)\mathbf{c} \tag{A.19}$$

where the vectors

$$\mathbf{s}(\xi) = \left\{\sin\lambda_1\xi, \cos\lambda_1\xi, \sin\widehat{\lambda}_2\xi, \cos\widehat{\lambda}_2\xi\right\}^T \tag{A.20}$$

and

$$\mathbf{c} = \{c_1, c_2, c_3, c_4\}^T. \tag{A.21}$$

Applying the boundary conditions in Table 1 on the expression of $W(\xi)$ in (A.19) and following similar procedure as the previous case, the frequency equation can be expressed as

$$\begin{aligned}
&\Big(\cos(\lambda_1)\lambda_1\cos\Big(\widehat{\lambda}_2\Big)\hat{\lambda}_2^3 - \lambda_1\hat{\lambda}_2^3 - \lambda_1^3\widehat{\lambda}_2 + \cos(\lambda_1)\lambda_1^3\cos\Big(\widehat{\lambda}_2\Big)\lambda_2 + 2\ \sin(\lambda_1)\lambda_1^2\sin\Big(\widehat{\lambda}_2\Big)\hat{\lambda}_2^2\Big)\tilde{\nu}\\
&\quad + \Big(-\Omega^4\beta\ \sin(\lambda_1)\lambda_1^2\sin\Big(\widehat{\lambda}_2\Big) + \cos(\lambda_1)\lambda_1^3\Omega^2\sin\Big(\widehat{\lambda}_2\Big) - 2\ \lambda_1\Omega^4\cos(\lambda_1)\beta\ \cos\Big(\widehat{\lambda}_2\Big)\widehat{\lambda}_2\\
&\quad + 2\ \lambda_1\Omega^4\beta\ \widehat{\lambda}_2 - \lambda_1\Omega^2\cos(\lambda_1)\sin\Big(\widehat{\lambda}_2\Big)\hat{\lambda}_2^2 + \Omega^2\sin(\lambda_1)\cos\Big(\widehat{\lambda}_2\Big)\hat{\lambda}_2^3 - \sin(\lambda_1)\lambda_1^2\widehat{\lambda}_2\Omega^2\cos\Big(\widehat{\lambda}_2\Big)\\
&\quad -\Omega^4\sin(\lambda_1)\beta\ \sin\Big(\widehat{\lambda}_2\Big)\hat{\lambda}_2^2\Big)\alpha - 2\ \cos(\lambda_1)\lambda_1^3\cos\Big(\widehat{\lambda}_2\Big)\hat{\lambda}_2^3 - \sin(\lambda_1)\lambda_1^4\sin\Big(\widehat{\lambda}_2\Big)\hat{\lambda}_2^2\\
&\quad - \sin(\lambda_1)\lambda_1^2\sin\Big(\widehat{\lambda}_2\Big)\hat{\lambda}_2^4 + {\lambda_1}^5\widehat{\lambda}_2 - \Omega^2\beta\ \cos(\lambda_1)\lambda_1\sin\Big(\widehat{\lambda}_2\Big)\hat{\lambda}_2^4 + \Omega^2\beta\ \sin(\lambda_1)\lambda_1^2\cos\Big(\widehat{\lambda}_2\Big)\hat{\lambda}_2^3\\
&\quad - \sin(\lambda_1)\lambda_1^4\Omega^2\beta\ \cos\Big(\widehat{\lambda}_2\Big)\widehat{\lambda}_2 + \cos(\lambda_1)\lambda_1^3\Omega^2\beta\ \sin(\lambda_2)\hat{\lambda}_2^2 + \lambda_1\hat{\lambda}_2^5 = 0.
\end{aligned} \tag{A.22}$$

The natural frequencies can be obtained by solving Eq. (A.22) for Ω. Again, due to the complexity of this transcendental equation it should be solved numerically.

Appendix B. Determination of the stiffness correction factor

We express Eq. (23) as

$$W(\xi) = \mathbf{s}^T(\xi)\mathbf{c}$$

where the vectors

$$\mathbf{s}(\xi) = \left\{\sin\lambda_1\xi\ \sinh\lambda_2\xi,\ \cos\lambda_1\xi\ \sinh\lambda_2\xi,\ \sin\lambda_1\xi\ \cosh\lambda_2\xi,\ \cos\lambda_1\xi\ \cosh\lambda_2\xi\right\}^T \tag{B.1}$$

and

$$\mathbf{c} = \{c_1, c_2, c_3, c_4\}^T. \tag{B.2}$$

Applying the boundary conditions in Table 2 on the expression of $W(\xi)$ in (B.1) we have

$$\mathbf{Q}\,\mathbf{c} = \mathbf{f} \tag{B.3}$$

where

$$\mathbf{f} = \begin{Bmatrix} 0 \\ 0 \\ 0 \\ -\frac{FL^3}{EI} \end{Bmatrix} \tag{B.4}$$

and the matrix

$$\mathbf{Q} = \begin{bmatrix} s_1(0) & s_2(0) & s_3(0) & s_4(0) \\ s_1'(0) & s_2'(0 & s_3'(0) & s_4'(0) \\ s_1''(1) & s_1''(2) & s_1''(3) & s_1''(4) \\ s_1'''(1) - \nu s_1'(1) & s_2'''(1) - \nu s_2'(1) & s_3'''(1) - \nu s_3'(1) & s_4'''(1) - \nu s_4'(1) \end{bmatrix} \tag{B.6}$$

The expression of $\mathbf{Q}$ can be obtained by substituting the functions $s_j(\xi)$, $j = 1, \ldots, 4$ from Eq. (B.2). The constants c_j can be obtained from Eq. (B.4) as

$$\mathbf{c} = \mathbf{Q}^{-1}\mathbf{f} \tag{B.7}$$

The deflection at the free end δ_L can be obtained by substituting $\xi = 1$ in Eq. (B.1) as

$$\delta_L = W(1) = \mathbf{s}^T(1)\mathbf{c} = \mathbf{s}^T(1)\mathbf{Q}^{-1}\mathbf{f} \tag{B.8}$$

The equivalent stiffness k_e can be obtained using

$$k_e = \frac{F}{\delta_L} = \frac{F}{\left(\mathbf{s}^T(1)\mathbf{Q}^{-1}\mathbf{f}\right)}$$

and consequently the stiffness correction factor defined in Eq. (15) can be calculated from

$$\gamma_k = \frac{k_e}{k_{CL}} = \frac{F}{\delta_L}\frac{L^3}{3EI} \tag{B.10}$$

Substituting the functions $s_j(\xi), j = 1, \ldots, 4$ from Eq. (B.2) into the expression of $\mathbf{Q}$ in Eq. (B.6) and simplifying we obtain the expression in Eq. (25). It is interesting to consider some special cases:

- *No axial force*, $\nu = 0$:
  This is the case of a beam resting of elastic foundation considered by [26] is considerable details. Substituting $\nu = 0$ in Eq. (31) one obtains

  $$\lambda_1 = \lambda_2 = \sqrt{\sqrt{\frac{\eta}{4}}} = \sqrt[4]{\frac{\eta}{4}} = \lambda \quad \text{(say)} \tag{B.11}$$

  Substituting $\lambda_1 = \lambda_2 = \lambda$ and $\nu = 0$ in Eq. (34) we get back the special case obtained by [26]

  $$\gamma_H = 2/3\ \frac{\lambda^3(\cosh(2\ \lambda) + \cos(2\ \lambda) + 2)}{\sinh(2\ \lambda) - \sin(2\ \lambda)} \tag{B.12}$$

- *No axial force and support stiffness*, $\nu = 0, \eta = 0$:
  This is the classical case of a simple cantilever beam and expect the stiffness correction factor to be 1. Substituting the expression of λ from Eq. (B.11) into Eq. (B.12) one obtains

  $$\gamma_H = 1/6\ \frac{\sqrt{2}\eta^{3/4}\left(\cosh\left(\sqrt{2}\sqrt[4]{\eta}\right) + \cos\left(\sqrt{2}\sqrt[4]{\eta}\right) + 2\right)}{\sinh\left(\sqrt{2}\sqrt[4]{\eta}\right) - \sin\left(\sqrt{2}\sqrt[4]{\eta}\right)} \tag{B.13}$$

  Now taking the limit $\eta \to 0$ we have

  $$\lim_{\eta\to 0}\ \gamma_H = \lim_{\eta\to 0}\ 1/6\ \frac{\sqrt{2}\eta^{3/4}\left(\cosh\left(\sqrt{2}\sqrt[4]{\eta}\right) + \cos\left(\sqrt{2}\sqrt[4]{\eta}\right) + 2\right)}{\sinh\left(\sqrt{2}\sqrt[4]{\eta}\right) - \sin\left(\sqrt{2}\sqrt[4]{\eta}\right)} = 1 \tag{B.14}$$

Case 2: $\eta < \left(\frac{\nu}{2}\right)^2$
In view of the roots in Eq. (26) the solution $W(\xi)$ can be expressed as

$$W(\xi) = c_1 \sin\ \lambda_1\xi + c_2 \cos\ \lambda_1\xi + c_3 \sin\ \hat{\lambda}_2\xi + c_4 \cos\hat{\lambda}_2\xi$$

or

$$W(\xi) = \mathbf{s}^T(\xi)\mathbf{c} \tag{B.15}$$

where the vectors

$$\mathbf{s}(\xi) = \left\{\sin\lambda_1\xi, \cos\lambda_1\xi, \sin\hat{\lambda}_2\xi, \cos\hat{\lambda}_2\xi\right\}^T \tag{B.16}$$

and

$$\mathbf{c} = \{c_1, c_2, c_3, c_4\}^T \tag{B.17}$$

Applying the boundary conditions in Table 2 on the expression of $W(\xi)$ in Eq. (B.15) and following the procedure similar to the previous case we have the expression in Eq. (30).

Appendix C. Determination of the mass correction factor

In view of the four roots given by Eq. (35), the solution of Eq. (33) can be expressed as

$$W(\xi) = c_1 \sin\ \hat{\eta}\xi\ \sinh\ \hat{\eta}\xi + c_2 \cos\ \hat{\eta}\xi\ \sinh\ \hat{\eta}\xi + c_3\ \sinh\ \hat{\eta}\xi \cos\ \hat{\eta}\xi + c_4 \cos\ \hat{\eta}\xi\ \cosh\ \hat{\eta}\xi \textit{ Break} \quad \text{or}$$
$$W(\xi) = \mathbf{s}^T(\xi)\mathbf{c} \tag{C.1}$$

where the vectors

$$\mathbf{s}(\xi) = \{\sin\hat{\eta}\xi\ \sinh\hat{\eta}\xi,\ \cos\hat{\eta}\xi\ \sinh\hat{\eta}\xi,\ \sin\hat{\eta}\xi\ \cosh\hat{\eta}\xi,\ \cos\hat{\eta}\xi\ \cosh\hat{\eta}\xi\}^T \tag{C.2}$$

and

$$\mathbf{c} = \{c_1, c_2, c_3, c_4\}^T \tag{C.3}$$

Applying the boundary conditions given after Eq. (33) on the expression of $W(\xi)$ in (C.1) we have

$$\mathbf{Q}\,\mathbf{c} = \mathbf{f} \tag{C.4}$$

where

$$\mathbf{f} = \begin{Bmatrix} 0 \\ 0 \\ 0 \\ 1 \end{Bmatrix} \tag{C.5}$$

and the matrix

$$\mathbf{Q} = \begin{bmatrix} s_1(0) & s_2(0) & s_3(0) & s_4(0) \\ s_1'(0) & s_2'(0) & s_3'(0) & s_4'(0) \\ s_1''(1) & s_2''(1) & s_3''(1) & s_4''(1) \\ s_1(1) & s_2(1) & s_3(1) & s_4(1) \end{bmatrix} \tag{C.6}$$

The expression of $\mathbf{Q}$ can be obtained by substituting the functions $s_j(\xi)$, $j = 1, \ldots, 4$ from Eq. (C.2) as

$$\mathbf{Q} = \begin{bmatrix} 0 & 0 & 0 & 1 \\ 0 & \hat{\eta} & \hat{\eta} & 0 \\ 2\cos(\hat{\eta})\hat{\eta}^2\cosh(\hat{\eta}) & -2\sin(\hat{\eta})\hat{\eta}^2\cosh(\hat{\eta}) & 2\cos(\hat{\eta})\hat{\eta}^2\sinh(\hat{\eta}) & -2\sin(\hat{\eta})\hat{\eta}^2\sinh(\hat{\eta}) \\ \sin(\hat{\eta})\sinh(\hat{\eta}) & \cos(\hat{\eta})\sinh(\hat{\eta}) & \sin(\hat{\eta})\cosh(\hat{\eta}) & \cos(\hat{\eta})\cosh(\hat{\eta}) \end{bmatrix} \tag{C.7}$$

The constants c_j can be obtained from Eq. (C.4) as

$$\mathbf{c} = \mathbf{Q}^{-1}\mathbf{f} \tag{C.8}$$

Considering harmonic motion the kinetic energy of the beam can be obtained as

$$\begin{aligned} T &= \frac{\omega^2}{2}\int_0^L mW^2(x)\,dx + \frac{\omega^2}{2}MW^2(L) \\ &= mL\frac{\omega^2}{2}\int_0^1 W^T(\xi)W(\xi)\,d\xi + \frac{\omega^2}{2}M1^2 \\ &= mL\frac{\omega^2}{2}\int_0^1 \mathbf{c}^T\mathbf{s}(\xi)\mathbf{s}^T(\xi)\mathbf{c}\,d\xi + \frac{\omega^2}{2}M \\ &= \frac{\omega^2}{2}(mL\gamma_m + M) \end{aligned} \tag{C.9}$$

where the mass correction factor is given by

$$\gamma_m = \int_0^1 \mathbf{c}^T\mathbf{s}(\xi)\mathbf{s}^T(\xi)\mathbf{c}\,d\xi \tag{C.10}$$

Evaluating this integral we have Eq. (36).

References

[1] Abdoun TH, Dobry R. Evaluation of pile foundation response to lateral spreading. Soil Dynamics and Earthquake Engineering 2002(22):1051–8.
[2] Abdoun T, Dobry R, O'Rourke TD, Goh SH. Pile response to lateral spreads: centrifuge modeling. Journal of Geotechnical and Geoenvironmental Engineering 2003;129(10):869–78.
[3] Abdoun TH. Modelling of seismically induced lateral spreading of multilayered soil and its effect on pile foundations. PhD thesis, Rensselaer Polytechnic Institute, NY. 1997.
[4] Adhikari S, Bhattacharya S. Dynamic Instability of pile-supported structures in Liquefiable soils during earthquakes. Shock and Vibration 2008;15(6): 665–85.
[5] AIJ, Architectural Institute of Japan, Recommendations for design of building foundations, (in Japanese), 1988, 2001.
[6] Anderson AW, Blume JA, Degenkolb HJ, Hammill HB, Knapik EM, Marchand HL, Powers HC, Rinne JE, Sedgwick GA, Sjoberg HO. Lateral forces of earthquake and wind. Transactions of the ASCE 1952;117:716–80.
[7] API, American Petroleum Institute, Recommended practice for planning designing and constructing fixed offshore platforms, 2003.
[8] Berrill JB, Christensen SA, Keenan RP, Okada W, Pettinga JR. Case studies of lateral spreading forces on a piled foundation. Geotechnique 2001;51(6): 501–17.
[9] Bhattacharya S, Adhikari SA. A rigorous analytical modelling of vibration of a pile-supported structure in liquefied soil during earthquakes. Geotechnique, 2009, in preparation.
[10] Bhattacharya S, Madabhushi SPG. A critical review of methods of pile design in seismically liquefiable soils. Bulletin of Earthquake Engineering 2008;6(3):407–47.
[11] Bhattacharya S. Pile instability during earthquake liquefaction, PhD thesis, University of Cambridge (UK), 2003.
[12] Bhattacharya S, Madabhushi SPG, Bolton MD. An alternative mechanism of pile failure in liquefiable deposits during earthquakes. Geotechnique 2004;54(April issue, No.3):203–13.
[13] Bhattacharya S, Bolton MD, Madabhushi SPG. A reconsideration of the safety of the piled bridge foundations in liquefiable soils. Soils and Foundations 2005;45(August issue, No. 4):13–26.
[14] BTL Committee, Study on liquefaction and lateral spreading in the 1995 Hyogoken-Nambu earthquake, Building Research Report No 138, Building Research Institute, Ministry of Construction, Japan (in Japanese), 2000.
[15] Blevins RD. Formulas for natural frequency and mode shape. Malabar, FL, USA: Krieger Publishing Company; 2001.
[16] Dash SR, Bhattacharya S, Blakeborough A, Hyodo M. P–Y curve to model lateral response of pile foundations in liquefied soils, Paper number 04-01-0089. In: Proceedings of the 14th World Conference on Earthquake Engineering, October 12–17, 2008, Beijing, 2008.
[17] DnV: Det Norske Veritas Code: Recommeded Practice for Foundation Design.
[18] Dobry R, Abdoun T, O'Rourke TD, Goh SH. Single piles in lateral spreads: field bending moment evaluation. Journal of Geotechnical and Geoenvironmental Engineering, ASCE 2003;129(10):879–89.
[19] Dobry R, Abdoun T. Recent studies on seismic centrifuge modelling of liquefaction and its effect on deep foundation. In: Proceedings of the 4th International Conference on Recent Advances in Geotechnical Earthquake Engineering and Soil Dynamics and Symposium in Honour of Professor W.D. Liam Finn, San Diego, California, March 26–31, 2001.
[20] Eurocode 8, Design provisions for earthquake resistance of structures—foundations, retaining structures and geotechnical aspects. European Committee for Standardization, Brussels, 1998.
[21] Finn WDL, Thavaraj T. Deep foundations in liquefiable soils: case histories, centrifuge tests and methods of analysis. In: Proceedings of the 4th International Conference on Recent Advances in Geotechnical Earthquake Engineering and Soil Dynamics and Symposium in Honour of Professor W.D. Liam Finn, San Diego, California, March 26–31, 2001.
[22] He Liangcai, Elgamal A, Abdoun T, Abe A, Dobry R, Meneses J, Sato M, Tokimatsu K. Lateral load on piles due to liquefaction-induced lateral spreading during one-G shake table experiments. In: Proceedings of the 100th Anniversary Earthquake Conference Commemorating the 1906 San Francisco Earthquake, April 18–22, California, 2006.
[23] Hamada M. Performances of foundations against liquefaction-induced permanent ground displacements. In: Proceedings of the 12th World Conference on Earthquake Engineering, Auckland, New Zealand, paper no. 1754, 2000.
[24] Hamada M. Large ground deformations and their effects on lifelines: 1964 Niigata earthquake. Case studies of liquefaction and lifelines performance during past earthquake. Technical Report NCEER-92-0001, Volume-1, Japanese Case Studies, National Centre for Earthquake Engineering Research, Buffalo, NY, 1992a.
[25] Hamada M. Large ground deformations and their effects on lifelines: 1983 Nihonkai-Chubu earthquake. Case studies of liquefaction and lifelines performance during past earthquake. Technical Report NCEER-92-0001, Volume-1, Japanese Case Studies, National Centre for Earthquake Engineering Research, Buffalo, NY, 1992b.
[26] Hetenyi M. Beams on elastic foundation: theory with applications in the fields of civil and mechanical engineering. Ann Arbor, MI, USA: University of Michigan Press; 1946.
[27] Ishihara K. Terzaghi oration: geotechnical aspects of the 1995 Kobe earthquake. In: Proceedings of ICSMFE, Hamburg, 1997, p. 2047–73.
[28] JRA, Japanese Road Association, Specification for highway bridges, part V, seismic design, 2002, 1996.
[29] Kimura Y, Tokimatsu K. Buckling stress of slender pile with lateral displacement at the pile head in liquefied soils. Journal of Structural and Construction Engineering, AIJ (Architectural Institute of Japan) 2007(617): 169–75.
[30] Knappett JA, Madabhushi SPG. Modelling of liquefaction-induced instability in pile groups. ASCE Geotechnical Special Publication no. 145 on Seismic Performance and Simulation of Pile Foundations in Liquefied and Laterally Spreading Ground, (Boulanger and Tokimatsu Eds.), 2005. pp. 255–67.
[31] Lin, et al. Damage of piles caused by lateral spreading—back study of three cases. ASCE Geotechnical Special Publication no. 145 on Seismic Performance and Simulation of Pile Foundations in Liquefied and Laterally Spreading Ground, (Boulanger and Tokimatsu Eds.), 2005.
[32] Liu L, Dobry R. Effect of liquefaction on lateral response of piles by centrifuge model tests. NCEER Report to FHWA. NCEER Bulletin, January 1995, Vol. 9(1).
[33] Mylonakis G. Simplified model for seismic pile bending at soil layer interfaces. Soils and Foundations 2001;41(4):47–58.
[34] Novak M, Nogami T, Aboul-Ella F. Dynamic soil reaction for plane-strain case. Journal of Engineering Mechanics Division, ASCE 1978;104(4):953–9.
[35] Rossett JM. Soil amplification of earthquakes. In: Desai CS, Christian JT, editors. Numerical methods in geotechnical engineering. New York: McGraw-Hill; 1977. p. 639–82.
[36] Rollins KM, Gerber TM, Dusty LJ, Ashford SA. Lateral resistance of a full-scale pile group in liquefied sand. Journal of Goetechnical and Geoenvironmental Engineering, ASCE 2005;131(1).
[37] RTRI: Rail Technical Research Institute code—1999 edition.
[38] Takahashi A, Kuwano J, Arai Y, Yano A. Lateral resistance of buried cylinder in liquefied sand. In: Proceedings of The International Conference on Physical Modelling in Geotechnics, ICPMG-02, St. Johns, Newfoundland, Canada, July 2002.
[39] Thomson JMT, Hunt GW. Elastic instability phenomenon. Chichester: Wiley; 1984.
[40] Tokimatsu K, Oh-oka Hiroshi, Satake K, Shamoto Y, Asaka Y. Failure and deformation modes of piles due to liquefaction-induced lateral spreading in the 1995 Hyogoken-Nambu earthquake. Journal of Structural and Construction Engineering, AIJ (Japan) 1997(495):95–100.
[41] Tokimatsu K, Mizuno H, Kakurai M. Building damage associated with geotechnical problems. Special Issue of Soils and Foundations, Japanese Geotechnical Society 1996:219–34.
[42] Uzuoka R, Sento N, Yashima A, Zhang F. 3-dimensional effective stress analysis of a damaged group-pile foundation adjacent to a quay wall. Journal of Japanese Association for Earthquake Engineering, JAEE 2002.
[43] Yasuda S, Terauchi T, Morimoto H, Erken A, Yoshida N. Post liquefaction behaviour of several sands. In: The 11th European Conference on Earthquake Engineering. Rotterdam: Balkema; 1998, ISBN 90 5410 982 3.
[44] Yoshida N, Towahata I, Yasuda S, Kanatani M. Discussion to the paper by Bhattacharya et al. (2004) on "An alternative mechanism of pile failure in liquefiable deposits during earthquakes". Geotechnique 2005;55(3):259–63.
[45] Yoshida N, Hamada M. Damage to foundation piles and deformation pattern of ground due to liquefaction-induced permanent ground deformation. In: Proceedings of 3rd Japan–US workshop on Earthquake Resistant Design of Lifeline Facilities and Countermeasures for Soil Liquefaction, 1990, p. 147–61.
[46] Shanker K, Basudhar PK, Patra NR. Buckling of piles under liquefied soil conditions. Geotechnical and Geological Engineering 2007;25(3).
[47] Dash SR, Raju LG, Bhattacharya S. A case study of damages of the Kandla Port and Customs office tower supported on a mat-pile foundation in liquefied soils under the 2001 Bhuj earthquake. Soil Dynamics and Earthquake Engineering 2009;29(2):333–46.
[48] Bhattacharya S, Blakeborough A, Dash SR. Learning from collapse of piles in liquefiable soils. In: Proceedings of the institution of civil engineers, Civil Engineering 161, No. CE6; November 2008. p. 54-60.
[49] Terzaghi K. Evaluate of coefficient of subgrade reaction. Géotechnique 1955;4:186–215.